Journal of Applied Fluid Mechanics, Vol. 9, No. 6, pp. 2695-2705, 2016.
Available online at www.jafmonline.net, ISSN 1735-3572, EISSN 1735-3645.
DOI: 10.29252/jafm.09.06.25908

Investigation of the Rotor Wake of Horizontal Axis Wind Turbine under Yawed Condition

B. Noura[1†], I. Dobrev[2], R. Kerfah [1], F. Massouh[2] and S. Khelladi[2]

[1] *Laboratory FIMA University of Djillali Bounaama Khemis Miliana, Algeria*
[2]*Arts et Métiers Paris Tech, 151, Boulevard de l'Hôpital 75013 Paris, France*

†Corresponding Author Email: *nourabelhadj@yahoo.fr*

(Received November 21, 2015; accepted February 21, 2016)

ABSTRACT

The wake and the lack of existing velocity behind the wind turbine affect the energy production and the mechanical integrity of wind turbines downstream in the wind farms. This paper presents an investigation of the unsteady flow around a wind turbine under yawed condition. The simulations and experimental measures are made for the yaw angle rotor 30° and 0°. The wind velocity is 9.3 m/s and the rotation velocity rotor of the wind turbine in 1300, 1500 and 1800 rpm. The wind turbine rotor which is modeled is of a commercial wind turbine i.e. Rutland 503. The approach Improved Delayed Detached Eddy Simulation (IDDES) based on the SST turbulence model is used in the modeling of the flow. The solutions are obtained by using the solver which uses finite volume method. The particle image velocimetry (PIV) method is used in wind tunnel measurements in the experimental laboratory of the ENSAM Paris-Tech. The yawed downstream wake of the rotor is compared with that obtained by the experimental measurements. The results illustrate perfectly the development of the near and far wake of the rotor operation. It is observed that the upstream wind turbine yawed will have a positive impact on the power of the downstream turbine due the distance reduction of the downstream wake of the wind turbine. However the power losses are important for yawed wind turbine when compared with the wind turbine without yaw. The improved understanding of the unsteady environmental of the Horizontal Axis wind Turbine allows optimizing wind turbine structures and the number of wind turbines in wind farms.

Keywords: Wind Turbine; wake; Delayed Detached Eddy Simulation; Yawed.

NOMENCLATURE

C_P	power coefficient	ψ	yaw angle
D	rotor diameter	Θ	azimuthally angle
dt	time step	λ	the tip speed ratio TSR
f, g	generic functions	V_∞	infinite velocity
k	kinetic turbulence energy	α	angle of attack
N	rotational velocity	ω	dissipation rate frequency of k
		P	density

1. INTRODUCTION

Wind turbines offer the promise of inexpensive and clean energy, in recent years, due to the increasing demand for energy, there has been a rapid development of wind turbines. In order to minimize the costs of energy production, the wind turbines are grouped in farms. The distance between the machines is reduced and so the aerodynamic interference becomes significant, especially when a given wind turbine operates in the wake of another.

Generally, it is supposed that after a distance of 7 times the rotor diameter in the axial direction the influence of upstream wake on power generation becomes less at 20% see e.g. Barthelmie *et al*. (2009) and "Dahlberg *et al*. (2009)". In addition, the operating condition of wind turbine also depends on wind direction and wind velocity. It is impossible for the wind turbine to have the axis permanently aligned toward the wind direction, hence, the flow is often yaw, see Jourieh M. (2007). Under these conditions, the flow is very complex. The same for

minimizing the influence of the yawed wake on the downstream side wind turbine in the perpendicular direction to the wind direction, the distance used is usually 3 times the rotor diameter. However, these distances vary significantly if the turbines are installed in complex terrain or when the wind turbulence is different from the usual case.

In these situations, an investigation of flow downstream of the wind turbine will be particularly helpful. The results of such investigations permit to obtain an optimal placement of wind turbines in the wind farm and to avoid operating of some wind turbines in the wake of the others. The wake behind the wind turbine rotor is due to kinetic energy extraction by the rotor. There are two distinct regions in the wake: the near wake, immediately behind the rotor, where the individual presence of each rotor blade can be observed, and the far wake where the large-scale vortex structures become dominant. A growing number of researchers are using experimental investigation and computational fluid dynamics (CFD) to study wind-turbine wake aerodynamics because the simplified aerodynamic models used for wind farm design are not well adapted and cannot describe correctly the behavior of wind turbine rotor see Jourieh M. (2007).

In experimental investigations, a few researchers used method particle image velocimetry (PIV) technique for the analysis of wind turbine wake. This experimental measurement method (PIV) is a non-intrusive method that can measure the instantaneous velocity vector field in a plan. Amongst these investigations we might mention the papers presented by Grant and Parkin, (2000), Maeda, *et al*. (2005) and Massouh and Dobrev, (2007). More recent studies are presented by Sherry, *et al*. (2013). However, experimentally it is difficult to obtain a spatial and temporal resolution sufficient to explore the wake development at more distance. For the moment, the experiment in a large field velocity is out of the current resources. Accordingly the computational fluid dynamics (CFD) is an alternative and also a necessity for to study wind turbine wake aerodynamics.

Several authors have performed CFD computations at the National Renewable Energy Laboratory (NREL) unsteady aerodynamic experiment Fingersh *et al*. (2001) and Hand *et al*. (2011) with a variety of turbulence models. Sørensen *et al.* (2002) (with the SST k–ω model) and Johansen *et al*. (2002) (with DES) performed simulations of the NREL phase VI rotor with a rotor-fixed reference frame. Li *et al*. (2012) compared the NREL Phase VI tu rbine, using unsteady RANS and DES turbulence modeling. The turbulence was modeled, using the blended k–ε/k–ω Shear Stress Transport (SST) model. In the laboratory of the ENSAM Paris-Tech several numerical works was completed for the exploration of the wake rotor .Massuoh and Dobrev (2005-2007). In addition one can also quote a numerical work on the flow around the rotor wind it was realized by Troldborg and Sørensen (2008). In this work, they study the characteristics of wakes of wind turbines operating in various flow conditions including interacting wakes between a row of turbines.

The present work was motivated by the need to understand the development of the wake behind wind turbine in axial position and yawed. Therefore two case will be considered, one where the wind turbine is in yawed position at angle 30° and the case where the flow is axial for wind turbine (yaw angle= 0°). In the purpose of a quantity and qualitative assessment of the turbulent flow characteristics, we undertook a simulation of the three-dimensional unsteady flow and experimental measurements by PIV to validate the numerical results. The flow is modeled numerically using the Improved Delayed Detached Eddy Simulation (IDDES) computational method based on the Navier-Stokes equations with the SST closure turbulence model. Improved Delayed Detached-Eddy Simulation (IDDES) by Shur *et al* (2008) is an improved version of the original DES model. Initially, the DES concept has been proposed by Spalart (1999, 1997). The DES is hybrid solution between the Reynolds averaged Navier-Stokes (RANS) and Large Eddy Simulation (LES) methods.

A physical analysis of the flow is presented for two positions of the rotor. We began by analyzing the physics of unstable axial flow around the turbine rotor (yaw angle = 0). Then an analysis for the flow around a wind turbine yawed. Moreover, experimental measurements of the torque developed for different positions (yaw angle 30 ° and 0 °) of the wind turbine are compared with the numerical results obtained.

2. MATHEMATICAL MODEL

The Improved Delayed Detached Eddy Simulation (IDDES) model of Shur *et al*. (2008) is a hybrid RANS-LES model that provides a more flexible and convenient scale-resolving simulation (SRS) model for high Reynolds number flows. The complete formulation is relatively complex and has been implemented as published by Shur *et al*. (2008). The IDDES model implemented based on the SST model Similar to DES, the k-equation of the SST model is modified to include information on the local grid spacing. With IDDES, a blending function similar to the one used by Menter and Kuntz (1994) for the SST model is introduced to limit the length scale of DES 97 to ensure the transition of RANS to LES be independent of grid spacing. Spalart *et al*. (1999). The SST-IDDES model is based on modifying the sink term in the k-equation of the SST model is:

$$\frac{\partial(\rho k)}{\partial t}+\nabla.(\rho\tilde{U}k)=\nabla.[(\mu+\frac{\mu_T}{\rho_{k3}})\nabla k] + P_k-\rho\beta^* k\omega F_{IDDES} \quad (1)$$

$$\frac{\partial(\rho\omega)}{\partial t}+\nabla.(\rho\tilde{U}\omega)=\nabla.[(\mu+\frac{\mu_T}{\rho_{\omega 3}})\nabla\omega] + (1-F_1)2\rho\frac{\nabla k\nabla\omega}{\sigma_{\omega 2}\omega}+\alpha_3\frac{\omega}{k}P_k-\beta_3\rho\omega^2 \quad (2)$$

Were F_{IDDES} is based on the RANS turbulent length scale and the LES grid length scales.

$$F_{IDDES} = \frac{l_{RANS}}{l_{IDDES}} \quad \text{and} \quad l_{RANS} = \frac{\sqrt{k}}{\beta^* \omega} \tag{3}$$

Note in the DES formulation, turbulent boundary layer simulations, grid cells are anisotropic, and the length scale Δ is defined as the maximal length of the cell in the three directions ,

$$\Delta = \max(\Delta_x, \Delta_y, \Delta_z) \tag{4}$$

In the IDDES formulation, the sub-grid length scale Δ differs from the DES formulation, where it is equal to the maximum local edge length for the considered cell. In the IDDES formulation, instead of h_{max}, a more general formulation for Δ is used that combines local grid scales and the wall distance d_w. The Values h_{max} and h_{min} are the maximum and the minimum edge length of each cell, respectively. The complete formulation is relatively complex and has been implemented as published by Shur *et al* (2008).

3. GEOMETRY MODELING AND CALCULATION GRID

3.1- 3-D Modeling of the Rotor

The rotor modeled studied here is a commercial wind turbine i.e. Rutland 503 of the Marlec Company. This rotor was modified for the tests at the Aerodynamics Laboratory (LMF) of the ENSAM Paris-Tech. Fig. 1.a shows this three-bladed wind turbine similar to the wind turbines used in the firm wind turbine.

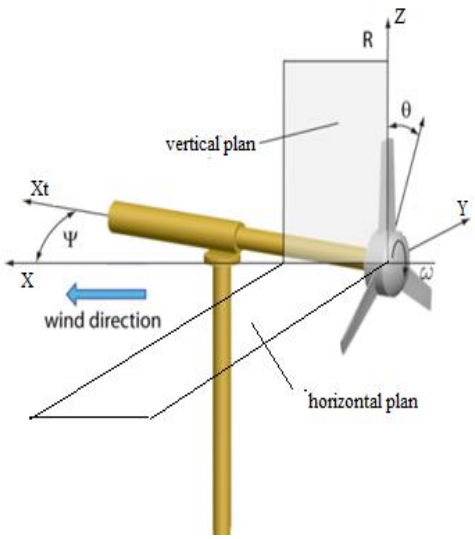

Fig. 1. a: Rotor in yaw position.

Figure 1.a shows also the wind turbine in yawed position with a designation of the investigation plans of the downstream wake (vertical and horizontal plane passing through the axis of rotation of the wind turbine). Fig. 1.b shows the experimental test bed PIV in the wind tunnel ENSAM which includes:

-The rotor of horizontal axe turbine Rutland 503 used and its equipment

-Wind Tunnel Laboratory LMA Arts and Métiers Paris-Tech

-chain of measurement by the method of Particle Image Velocimetry PIV.

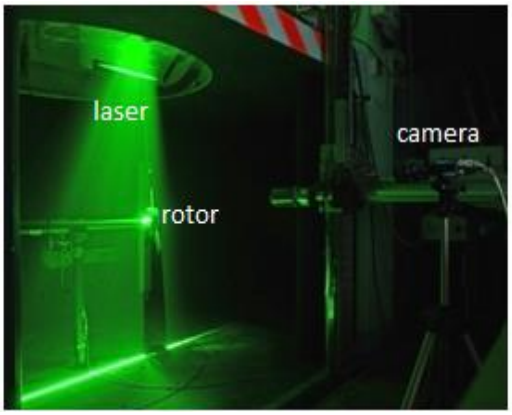

Fig. 1. b: chain of measurement by PIV.

Figure 2 show the geometrical basis parameters of the Rutland rotor. These parameters were taken accurately and digitized for a rotor with the hub. The blades are untwisted and are fitted with a constant pitch angle equal 10 degrees.

This geometry of the digitized rotor was used in order to generate fluid volumes which constitute the various fields of calculation.

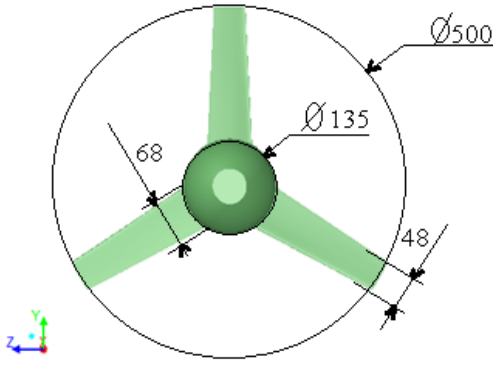

Fig. 2. Geometric parameters of the Rutland 503 rotor.

3.2- Calculation Grid

The modeling of the calculation grid is done through a 3-D system of coordinates of the actual model. The wind turbine tower and the ground are not included in the flow model.

To take into account the rotor rotation, the flow field is divided into two distinct zones of mesh: an external fluid field which is the wind flow tunnel and a field that represents the internal fluid the turbine rotor. Thus, we construct the computational domain by grouping the mesh of the two areas. Fig. 3a shows the mesh elements adopted for the computational model.

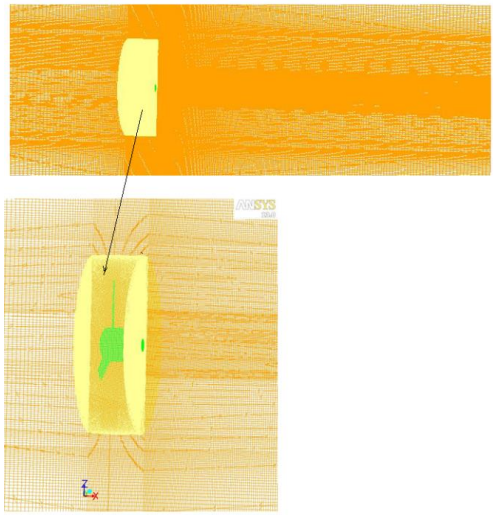

Fig. 3. a: domain mesh.

The structured grid generation was used for the geometrical calculation fields defined above. The mesh element sizes are controlled to obtain fine mesh elements close to the blades, hub and downstream of the rotor. Fig. 3 b shows a grid point distribution in Rotor surface. In order to resolve the strong gradients in the vicinity of the wind turbine rotor, a high concentration of grid points was distributed in the region downstream of the rotor, to account for the wake expansion. Accurate results can only be obtained using very fine mesh. The Solution seems to be independent from grid size has been obtained after many subsequent adaptations. The total number of hexahedral mesh after adapting is approximately 14 million volumes.

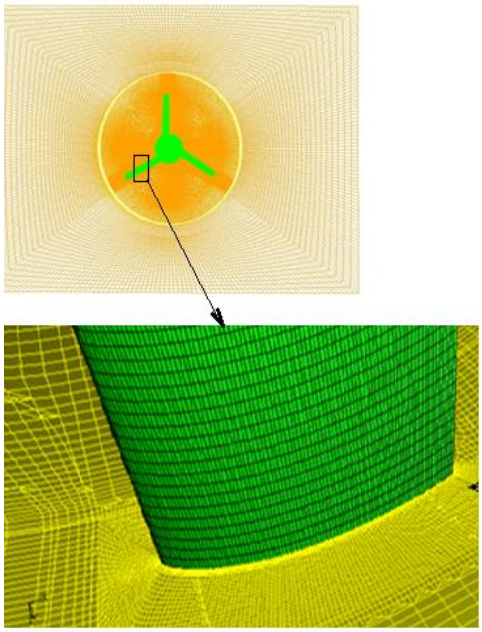

Fig. 3. b: Rotor surface mesh.

The single blade is divided within the cord direction into 90 intervals, which are slightly refined around the edges, where the gradient speed is strongest. In order to improve the grid of the boundary layer, 10 layers of mesh in the vicinity of the blades walls are used. Here, the initial size of the mesh in the normal direction is 0.15 percent of the cord and the growth promoter of 1.25 is used. To get an excellent grid, the entire domain was divided into 210 blocks.

The single blade is divided within the cord direction into 90 intervals, which are slightly refined around the edges, where the gradient speed is strongest. In order to improve the grid of the boundary layer, 10 layers of mesh in the vicinity of the blades walls are used. Here, the initial size of the mesh in the normal direction is 0.15 percent of the cord and the growth promoter of 1.25 is used. To get an excellent grid, the entire domain was divided into 210 blocks.

4. CALCULATION CONDITIONS

The computations presented in this paper have been obtained using a finite-volume method by Fluent commercial computational fluid dynamic package Fluent Ansys Inc (2010). The numerical analysis was performed under a 3-D incompressible unsteady state condition and applied the Improved Delayed Detached-Eddy Simulation (IDDES) method based on SST k-ω turbulent model.

The unsteady terms are implicit second-order discredited. A centered Simple algorithm is used for the pressure-velocity coupling and a third-order Muscl scheme discretization is used for the convection and diffusion terms. The inlet condition was set on the upwind face of the stator domain, imposing a constant wind profile equal to 9.3 m/s with stochastic turbulence of 5% of the free stream velocity. The static atmospheric pressure was imposed on the remaining surfaces of the model. The angular velocity was imposed together with the "moving mesh" setting. The time step was chosen in such a manner that, for each time step, the mesh will only rotate one cell-thus enhancing the continuity of the two domains (the stationary domain and the rotating domain which contains the actual turbine geometry). Time step size is of the order of 3. 10^{-4}s. The calculation conditions were set as follows; the upstream flow velocity V∞ is maintained constant at 9.3 m/s, while the wind turbine rotational speed varies 1300 rpm, 1500rpm and 1800 rpm. Thus, the Reynolds number calculated with blade-tip-chord and tip-peripheral velocity U varies roughly between 110,000 and 150,000. These values of tip speed ratio (TSR) were chosen in reference to experimental work Belkheir Noura *et al*. (2012) realized in the laboratory of ENSAM .The tip speed ration (TSR) is defined by the formula 5:

$$\lambda = \frac{\pi \times N \times D}{60 \times V_{\infty}} \tag{5}$$

N is the rotational velocity in rpm of the rotor and D is the rotor diameter.

The most widely used way of demonstrating the performance of a wind generator is to show the variation in the power coefficient (Cp) according to the variation of the TSR. The power coefficient is given by the formula 1.

$$C_p = \frac{P_{measured}}{P_{avialable}} \tag{6}$$

$P_{measured}$ is the power measured during the experiment. The $P_{measured}$ is obtained from the mechanical torque measured by the torque- meter and rotational velocity of rotor. $P_{avialable}$ being the available power and is defined by the formula 7.

$$P_{avialable} = \rho_{air} \times \frac{V_{\infty}^{3}}{2} \times A \tag{7}$$

ρair is the density of air. The temperature in the wind tunnel during the measurements is constant. A is the flow section of the test section of the wind tunnel. V_{∞} is the measured velocity of the flow in the wind tunnel.

5. MODE EXPERIMENTAL

Experiments are conducted in the wind tunnel of Arts and Métiers-Paris-Tech. This wind tunnel is a closed-circuit type and the flow velocity can reach 40 m/s. The nozzle between the settling chamber and the test section has a contraction ratio of 12.5. This ratio ensures a uniform velocity profile and a turbulence ratio less than 0.25%. The semi-open test section of the wind tunnel has a cross-section of 1.35 m x1.65 m and a length of 2 m. The static pressure in the test section is equal to atmospheric pressure. Hence, the upstream velocity only depends on the stagnation pressure in the settling chamber.

The rotor is mounted on a shaft (Fig. 1), the latter being coupled with an electric continuous current generator. The monitoring of the rotational velocity and load of the rotor is provided by a rheostat connected to the output of the generator powering the wind turbine. The coupling between the rotor shaft and the generator is done via a torque- meter that measures the mechanical torque and transmits a square signal for each degree. Fig. 4 show the Schema of measurement chain PIV.

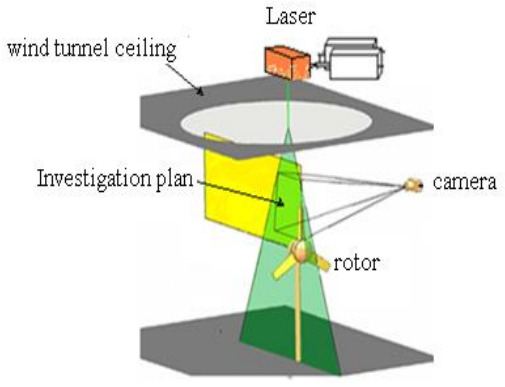

Fig. 4. Schema of measurement chain PIV.

A fiber-optic sensor is used to detect a reflective target fixed on the rotor shaft and thus to obtain a reference signal that informs about each blade pass. By counting the number of signals delivered by the torque-meter, after the passage of the reference signal, it is possible to obtain the rotor's angular position with an accuracy of 1°. Data acquisition is obtained using a data acquisition card that emits a TTL signal. This signal TTL or Transistor-Transistor Logic, which is a family of logic electronic circuits. This family of components combines good switching speed at a low transfer time. This signal is for triggering the PIV measurements at the desired angular position.

The PIV system is controlled by the software Dynamic Studio. The images are taken with use of an Nd-Yag 200 mJ laser, two cameras of 2048x2048 px equipped with the lens (Micro-Nikkor AF-S 105 mm f/2.8G IF-ED) and a system which synchronizes both image sensors and laser flashes with the blade angular position. The flow is seeded with micro-droplets of olive oil 2-5 μm of diameter, created by a mist generator.

A series of 500 pairs of images is taken from two cameras for each rotational speed. The blade tip is targeted by the first camera and the blade root is targeted by the second. The image capture is synchronized with the rotor position so the PIV system is triggered when the reference blade is positioned at the desired angular position, in this case when the reference blade is vertical. The laser sheet passes through the rotor axis and the axis of the reference blade.

The PIV region of interest is shown in Fig. 1. In this study, the yaw angle equal zero. Taking into account the frequency of the camera (7 Hz) the images are taken once every five or six revolutions. For each pair of images, the time delay between the first and second image is set to 40μs.This value has been established experimentally to ensure the best cross-correlation. The cross-correlation is applied to interrogation windows of 32x32 pixels and a 50% overlap, which results in a spatial resolution of 1.92 mm. Finally, the treatment of all PIV images permits to constitute a database including instantaneous and average velocity fields for each of the three rotational velocities.

6. RESULTS AND DISCUSSION

6.1 Analysis of the Structure Wake

Numerically it is possible to explore the rotor wash on a large field downstream, the field of study allows exploring approximately 7 times the radius of the rotor. Fig. 5 show the dimensionless Magnitude Velocity field in the vertical plane through the wind turbine center axis (y=R = 0), were R is the radius of rotor. The wake develops toward the downstream of the rotor model is presented in axial position (yaw angle=0) and at the TSR equal 3.63.

In experimental results, it is noteworthy that the review of successive fields over time shows a fluctuation in the position of the vortices cores relative to the plane of rotation. This fluctuation is due to the temporal variation of the rotor power. It may be noted that the radial fluctuation of the cores depends weakly on their axial positions. On the other hand, axial flutter increases rapidly, because this flutter is amplified by the number of steps taken.

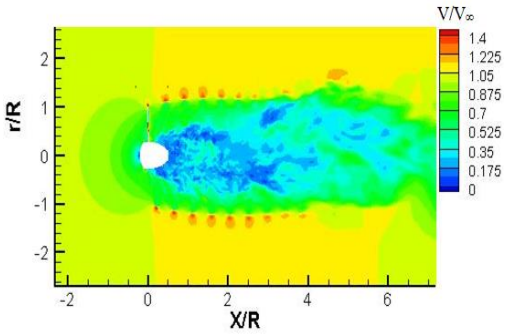

Fig. 5. Velocity field in the vertical plan, in yaw angle ψ=0 and TSR = 3.63.

Thus, comparing the average velocity obtained experimentally with those obtained numerically is a ideal solution. To get the experimental averaged velocity field, we averaged the resultant instantaneous field of series of images (200 images)

The wind that flows into the rotor generates a wake that develops toward the downstream due to the effect of the rotating rotor. The downstream flow is divided into two regions: an internal zone, where the wake is restrained and slowed by the tip vortices, and an external zone corresponding to a less-perturbed free flow.

In the internal zone, the wake generated also can be divided mainly into two distinct regions, a near wake and far wake region:

The near wake is taken as the region just behind the rotor, roughly up to 4 rotor radius downstream, it shows in Fig. 5. In the near wake, there are the central vortex that develops near the hub and the tip vortex that develops in the tip of the blade.

The far wake is a distance approximately equal to four times the radius of the rotor. At this distance the tip vortex breakdown occurs and then the wake becomes highly turbulent with irregular vortex structures. To understand the far wake development, it is necessary to have a good knowledge of the near wake structure immediately behind the rotor.

6.1.1 The Near Wake

The objective of this part of study is to investigate the near wake of the horizontal axis wind turbine while its tip-speed ratio (TSR) varies. Fig. 4 demonstrates the numerical results and the experimental measurements of the velocity fields that develops toward the downstream of the rotor in same position at yaw angle=0 (axial flow).

The experimental measured velocity fields are identical to the predicted velocity fields numerically. Magnitude velocity fields and vorticity fields for the 0° azimuth position are presented in Fig. 6-7-8.

FigureS 6 a-b-c-d shows the dimensionless magnitude velocity field and the vorticity field of numerical and experimental results at TSR 3.65 and Fig.7 a-b-c-d shows the dimensionless magnitude velocity field and the vorticity field of numerical and experimental results at TSR 4.22. Also Fig.8 a-b-c-d shows the dimensionless magnitude velocity field and the vorticity field of numerical and experimental results at TSR 5.06.

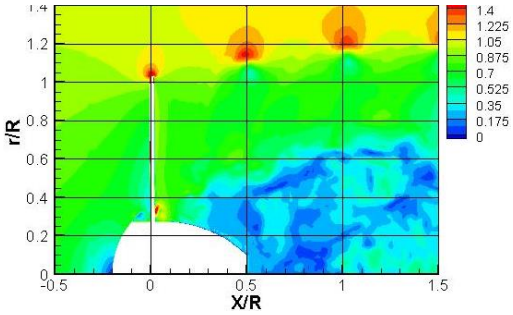

Fig. 6. a: Average velocity (numerical result) at TSR 3.65.

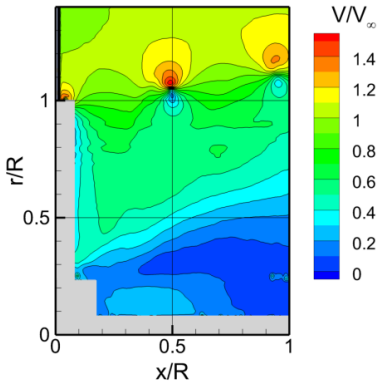

Fig. 6. b: Average velocity (experimental result) at TSR 3.65.

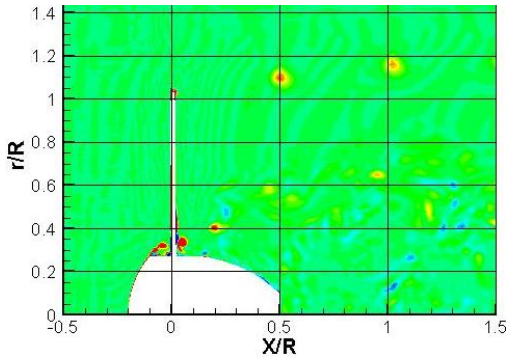

Fig. 6. c: Vorticity (numerical result) at TSR 3.65.

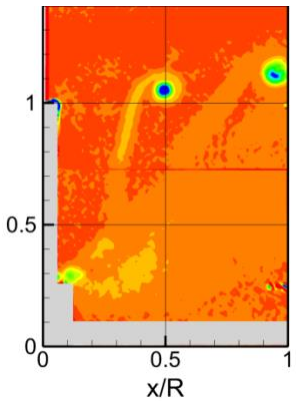

Fig. 6. d: Vorticity (experimental result) at TSR 3.65.

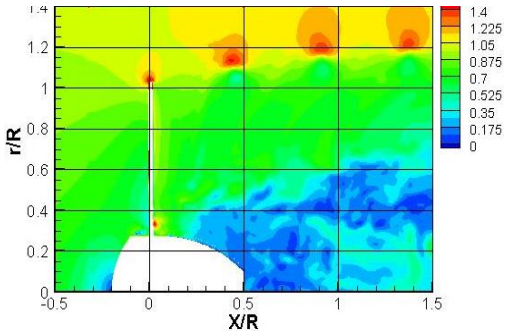

Fig.7. a: Average velocity (numerical result) at TSR 4.22.

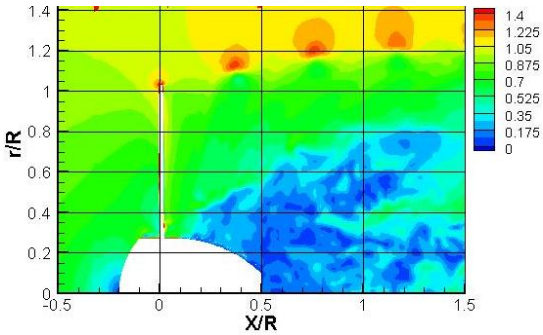

Fig. 8. a: Average velocity (numerical result) at TSR 5.06.

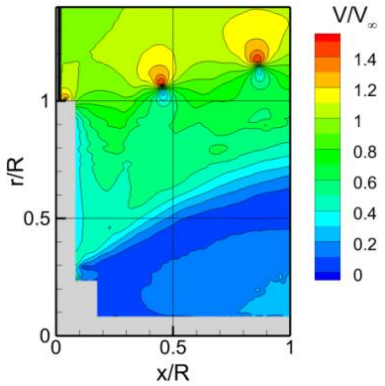

Fig. 7. b: Average velocity (experimental result) at TSR 4.22.

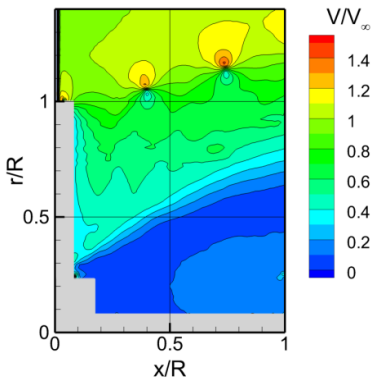

Fig. 8. b: Average velocity (experimental result) at TSR 5.06.

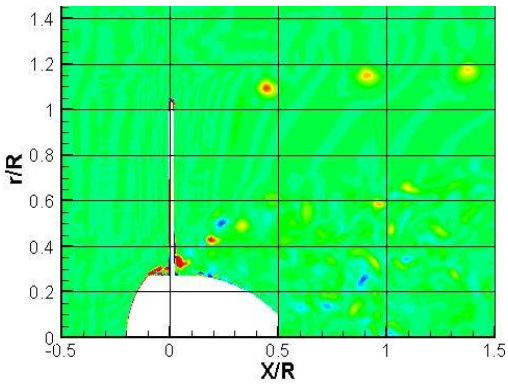

Fig. 7. c: Vorticity (numerical result) at TSR 4.22.

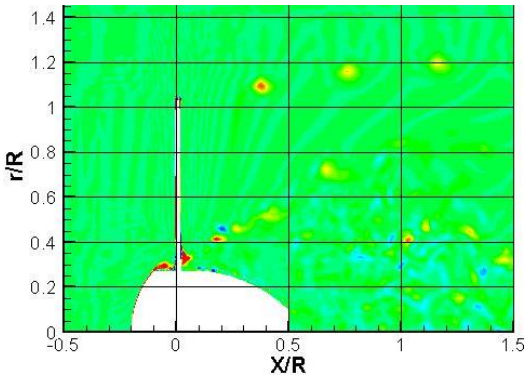

Fig. 8. c: Vorticity (numerical result) at TSR 5.06.

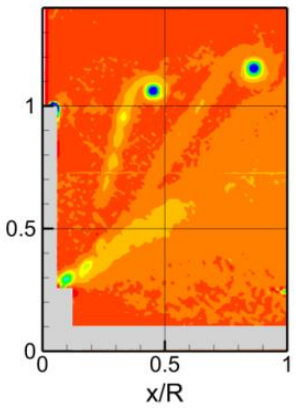

Fig. 7. d: Vorticity (experimental result) at TSR 4.22.

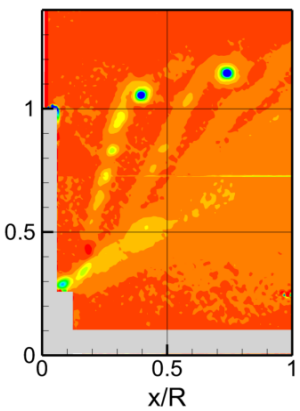

Fig. 8. d: Vorticity (experimental result) at TSR 5.06.

In these figures, the plane of exploration passes through the axis of rotation, where the reference blade is vertical. Experimental and numerical results show that the spiral geometry is maintained at a distance from the rotor.

Velocity field shows that the positions of the tip vortices are located where the velocity varies rapidly in the radial direction with a high gradient. These results show that at the core center of the vortex, the velocity varies with radius from values close to zero to values significantly higher than the upstream velocity.

The tip vortices trailing from the blades move with the fluid and as consequence, they have a helical shape. The plane of investigation cuts through these helixes and shows the vortex core as high velocity gradient. The first vortex represented on the left side of the images corresponds to the reference blade tip.

Figure 9 shows the spacing between the vortices for different rotational speed. The structure of the near wake that develops toward the backside of the rotor blade is so that the rotation speed of the rotor blade is faster; the space between the tip vortexes is narrower Faouaz Massouh *et al*. (2014). It is also known that it generates a fairly complicated structure of a 3-D vortex flow.

These vortices are also a major source of unsteadiness, aerodynamic noise and aerodynamic interaction. After a certain distance from the rotor, tip vortex breakdown occurs and then the wake becomes highly turbulent with irregular vortex structures.

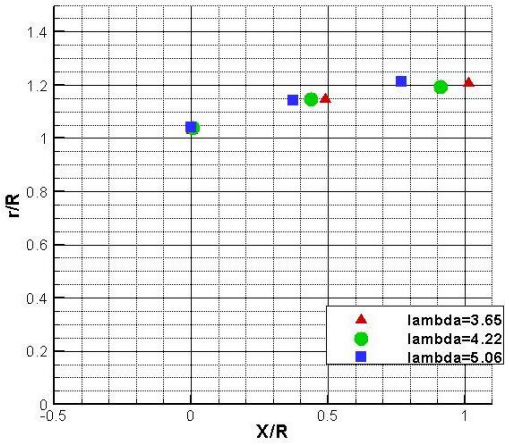

Fig. 9. Position of tip vortex core.

6.1.2- Far Wake

Figure 10 a-b-c show contours of the magnitude velocity in the vertical plane through the wind turbine center axis (x=R = 0) for each of the tested cases.

Figure 10 b-c shows for the rotor operating at the highest tip-speed ratio at λ=5.06 and 4.22 instability of the tip vortices is observed to appear only 2 rotor radii downstream and after 4 rotor radii the wake completely breaks up.

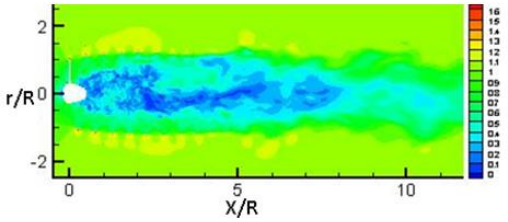

Fig. 10. a: velocity field at TSR 3.65.

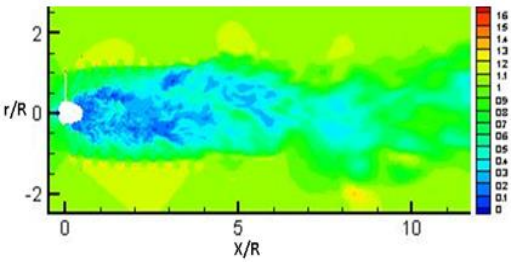

Fig. 10. b: velocity field at TSR 4.22.

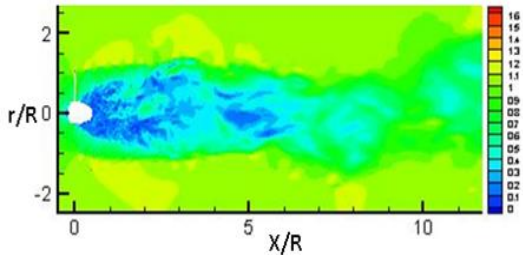

Fig. 10. c: velocity field at TSR 5.06.

Figure 10.a shows the case where λ = 3.65, the tip vortices are observed to undergo a Kelvin Helmholz instability approximately 6 rotor radii downstream. The root vortices become unstable at an earlier point (about 4 rotor radii downstream of the rotor) due to their proximity and further downstream the root and tip vortices interact, which causes the wake to become fully turbulent. In contrast to the two other cases, instability of the tip vortices does apparently not occur at λ = 3:65 due to the generally higher stability of the tip vortices, when the tip speed ratio and thus also the thrust is low.

As expected the wake of the rotor operating at λ= 5.06 differs quite significantly from the other situations by having hub vortices distributed over the entire radial extent of the wake. Moreover, the distributions of the hub vortices near the root at λ=3.65 to have a somewhat less large radial extent than at the higher tip speed ratios.

6.1.2- Near Yawed Wake.

The investigations are performed to show the influence of variation of yaw angle on the wake rotor downstream. The yaw angle chosen for these investigations is 30° with a wind turbine rotational speed of 1300 rpm and the wind speed 9.3 m/s matching TSR equal to 3.63. Fig. 12 a -b show a comparison between the near wake of an axial flow and the near yawed wake of wind turbine. We observed in the near yawed wake that the hub vortex increases in the size. The hub leads to blockage of the largest yaw flow compared to that of axial flow. Consequently, a significant slowdown will be behind

the hub, which gives a reason for the existence of larger aerodynamic interactions responsible for the power loss and noise generation.

Figure 12.b shows in the near yawed wake that variation of the tip vortex diameter is less important for the yawed wind turbine than the wind turbine with an axial flow. We can also see that the distance between two consecutive vortices tubes from the blade tips change significantly. This distance increases gradually.

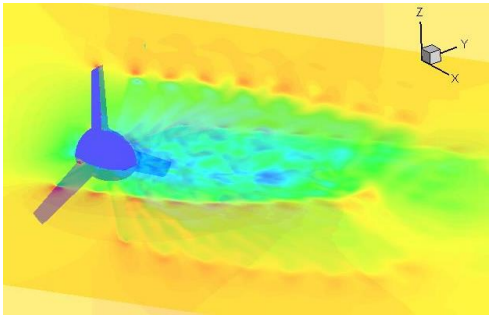

Fig. 11. a: Variation in the wake according to yaw angle in 3D.

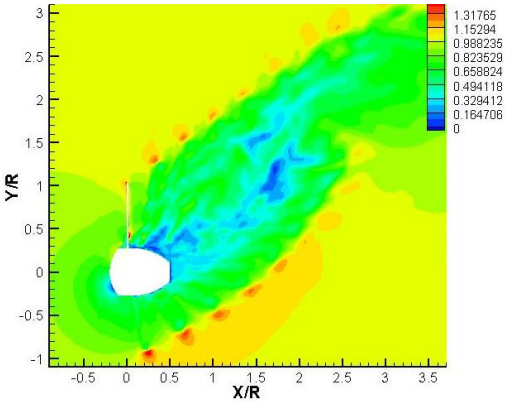

Fig. 11. b: Variation in the wake according to yaw angle in horizontal plan.

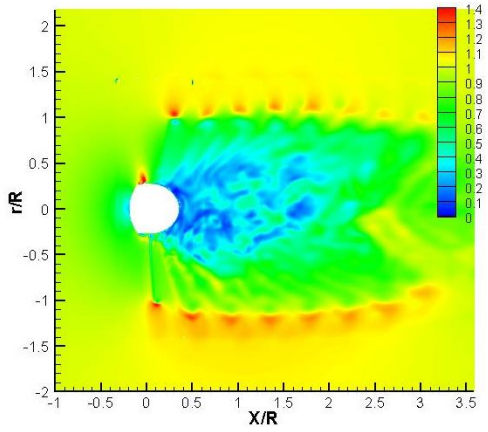

Fig. 11. c: Variation in the wake according to yaw angle in vertical plan.

6.1.3- The Far Yawed Wake

The objective of this part is to study how the far wake of yawed rotor decays downstream, in order to estimate the effects produced in downstream and near turbines. It was observed that yawing the upstream turbine has a positive impact on the power output from the downstream turbine AbdelSalam and Ramalingam (2014). The wind that flows into the rotor in yawed position generates a wake yaw that develops toward the downstream differently with respect to the wake of a wind turbine that operates in an axial position.

Figures 11a-b-c show contours of the axial velocity of numerical results obtained in the horizontal, vertical plane through the wind turbine center axis and in 3D.

Figure 11 b show in the horizontal plane, a very clear way the deviation of the wake on the near turbine in downstream. This deviation is to 1.5 radius of the rotor on the near wind turbine. Similarly we see the yaw wake develops over a distance equal to 4 times the radius of wind turbine. This wake grows at a lower distance than that of a the upstream wind turbine not yawed

By operating the upstream turbine at an appropriate yaw angle, one can use a relatively small distance of separation between the turbines. Therefore, operating the upstream turbine at a suitable yaw angle will reduce the space required for a given wind farm.

Figure 11.c shows also the tip vortices are observed to break downstream the rotor at 2.5 rotor radii in the same time as the root vortices, after the wake completely breaks up.

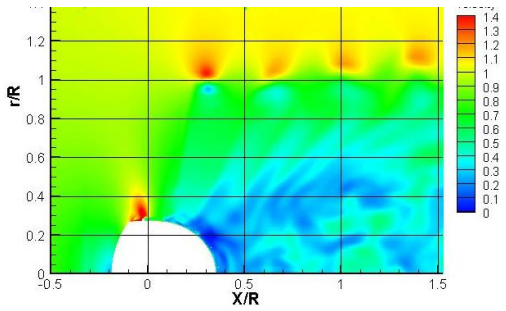

Fig. 12. a. Position of tip vortex core in yaw plan (Numerical result).

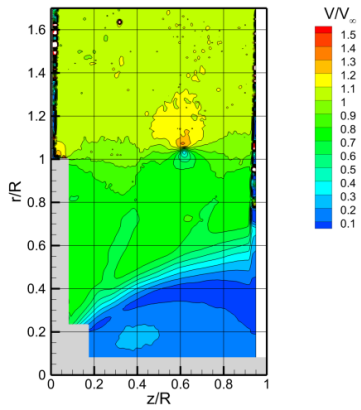

Fig. 12. b. Position of tip vortex core in yaw plan (Experimental result).

In numerical results one could obtain a mapping of the vortex line because the study area is large enough. Fig. 12 a shows the fields of velocity obtained numerically and Fig.12.b shows the fields of velocity obtained experimentally.

The field investigated experiment is limited because of the material used. Any time the position of two tip vortex is determined.

Figure 13 shows the predict position of the tip vortex line. The angle of yaw line drawn by the tip vortex core with the axis of rotor is approximately 36°.

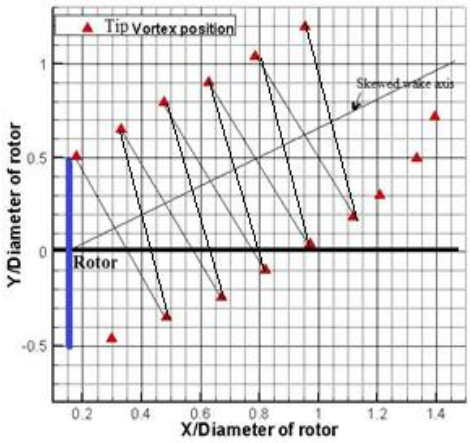

Fig. 13. Tip vortex position in yaw plan.

This angle is greater than the yaw angle; this result is confirmed by the results obtained by "Barthelmie RJ, Hansen K and al". (2009). The near wake in deflected in the direction perpendicular to the axis of rotation is at 1.5 times the rotor radius.

6.1- Comparison of Power Measurements of Wind Power

Table 1 shows the comparison of the power coefficient of the wind turbine model depending on the yaw angle for a value of about speed ratio 3.65. The maximum values of power coefficient are reached for a value of this tip speed ratio of around 0 .37 Belkheir Noura, Dobrev *et al*. (2012).

Experimental measurements give values of power coefficient lower of 7% compared to the values obtained numerically. The maximum power coefficient is 0.407 for axial flow (yaw angle=0°).

Table 1 Power coefficient

Yaw angle	Experimental CP	Numerical CP
0°	0.377	0.407
30°	0.265	0.293

This numerical power coefficient drops to a value of 0.293 or a loss of 28%. This is almost the same rate of loss power coefficient measured experimentally when the rotor is yawed. In reality, the power coefficient in the yaw position varies during each rotation of the rotor.

7. CONCLUSIONS

The far and near wake of a horizontal axis wind turbine were investigated numerically and experimentally for the turbine model Rutland 503. A commercial CFD code is used to predict the rotors wake of wind turbines and method PIV is used in experimental measurements. A complete overview of the flow field is given. The vortices of tip blades and hub rotor play an important role in the aerodynamics of the turbine. They produce a very complex flow field with strong gradients. These vortices are also the major source of instability. The results presented in this paper show the velocity deficit in the far wake, which propagates over a large distance, so that the downstream turbine sees freestream speed considerably lower than the upstream turbine and thus less energy is available in the stream. Therefore, the power losses to a turbine operating in the wake of another are significant.

The wake downstream of the rotor wind turbine in axial flow can attain a more distance. This wake for great value of TSR propagates over a large radial and axial distance. By adjusting the tip speed ratio of the upstream turbine, the power from the downstream turbine can be increased.

For a non-axial flow, the power output of wind turbine yawed drops significantly. However, It is also observed that the upstream wind turbine yawed will have a positive impact on the power of the downstream turbine due the distance reduction of the downstream wake of the wind turbine. By operating the upstream turbine at an appropriate yaw angle, one can use a relatively small distance of separation between the turbines. Therefore, operating the upstream turbine at a suitable yaw angle will reduce the space required for a given wind farm. But, there will be in counterpart a loss of the total power output of the wind farm. The overall efficiency of the wind farm was to be strongly dependent on the distance between the turbines and their operating conditions. By systematically controlling the operating conditions of the upstream wind turbine, the overall performance of a wind farm can be improved significantly.

ACKNOWLEDGEMENTS

I would like to thank Dr. Sofiane Khelladi for welcoming me in his team. I also thank Dr. Massouh for welcoming me in his Aerodynamics Laboratory of Arts ET Métiers School in Paris Tech., France.

REFERENCES

AbdelSalam, M., and V. Ramalingam (2014). Wake prediction of horizontal -axis wind turbine using full-rotor modeling. *Journal of Wind Engineering and Industrial Aerodynamics* volume 124 page 7–19.

Barthelmie, R. J., K. Hansen, S. T. Frandsen, O. Rathmann, J. G. Schepers, W. Schlez and *et al*. (2009). Modelling and measuring flow and wind turbine wakes in large wind farms

offshore. *Risø National Laboratory for Sustainable Energy Technical University of Denmark P.O.Box 49 DK-4000*. Report number Risø-R-1765(EN) . ISSN 0106-2840 ISBN 978-87-550-3878-3

Belkheir, N., I. Dobrev and *et al*. (2012) Experimental study of yawed inflow around wind turbine rotor. *Journal of Power and Energy* 226(5), 664–673.

Dahlberg, J. A. and S. E. Thor (2009). In *Proc. European Offshore Wind Conference and Exhibition*, Stockholm, Sweden.

Faouaz, M. and I. Dobrev (2005). Investigation of wind turbine near wake. *Int. Conf. on Jets, Wakes and Separated Flows*, Tobashi, Mie, Japan.

Faouaz, M. and I. Dobrev (2007). Exploration of the vortex wake behind of wind turbine rotor. *Journal of Physics: Conference Series* 75(1), 012036.

Faouaz, M. and I. Dobrev (2007). Exploration of the vortex wake behind of wind turbine rotor. *Journal of Physics: Conference Series* volume 75 numero (1),page 012036.

Faouaz, M. and I. K. Dobrev (2007). Exploration and numerical simulation of wind turbine wake. *Journal ISJAEE* .

Fingersh, L. J., D. Sinuns, M. M. Hand and D. Jager (2001).Wind tunnel testing of NREL's-unsteady aerodynamics experiment. In *Proceeding of ASME.*

Fluent Theory Guide ANSYS, Inc. Southpointe (2013) *275 Technology Drive Canonsburg, PA 15317*.

Grant, I. and P. Parkin, (2000).A DPIV study of the trailing vortex elements from the blades of a horizontal axis wind turbine in yaw. *Experiments in Fluids* Volume 28, issue 4,pages 368-376.

Hand, M. M., D. A. Simms, L. J. Fingersh and D. W. Jager (2001). Unsteady Aerodynamics Experiment PhaseVI: Wind Tunnel Test Configurations and Available Data Campaigns. *National Renewable Energy Laboratory*, Technical report Prepared under Task No. WER1.1110.

Ivan, D., B. Maalouf and N. Troldborg (2008). Investigation of the Wind Turbine Vortex Structure. *14th Int Symp on Applications of Laser Techniques to Fluid Mechanics*, Lisbon, Portugal.

Johansen, J., N. N. Sørensen, J. A. Michelsen and S. Schreck (2002). Detached-eddy simulation of flow around the NREL phase VI blade. *Wind Energy* 5, 185–197.

Jourieh, M. (2007). *Development of a representative of a wind turbine model to study the implementation of several machines on a wind farm*. Ph. D. thesis, Ecole Nationale Superieure d'Arts et Métiers Franch.

Li, Y., K. Paik, T. Xing and P. M. Carrica (2012). *Dynamic overset CFD simulations of wind turbine aerodynamics*.

Maeda, T., Y. Kinpara and T. Kakinaga (2005). Wind tunnel and field experiments on wake behind horizontal axis wind turbine, *Transactions of the Japan Society of Mechanical Engineers* 71(701), 162-170.

Menter, F. R. (1994) Two-Equation Eddy-Viscosity Turbulence Models for Engineering Applications. *AIAA Journal* 32(8), 1598–1605.

Sherry M., Sheridan J., Jacono D. L. (2013)"Characterisation of a horizontal axis wind turbine's tip and root vortices. *Experiments in fluids* volume 54 issue 3 page 1-19.

Shur, M. L., P. R. Spalart, M. K. Strelets and A. K. Travin (2008). A Hybrid RANS-LES Approach with Delayed-DES and Wall-Modelled LES Capabilities. *International Journal of Heat and Fluid Flow* 29(6), 1638-1649.

Sørensen, N. N., J. A. Michelsen and S. Schreck (2002). Navier–Stokes predictions of the NREL phaseVI rotor in the NASA Ames 80 ft_120ft wind tunnel. *Wind Energy* 5, 151–169.

Spalart, P. R., Jou, W-H., Strelets, M., and Allmaras, S. R., (1997), "Comments on the Feasibility of LES for Wings, and on a Hybrid RANS/LES Approach, Advances in DNS/LES", *1st AFOSR Int. Conf. On DNS/LES, Greyden Press, Columbus.*

Spalart, P. R., S. Deck, M. Shur and K. D. Squires. (2006). A New Version of Detached-Eddy-Simulation, Resistant to Ambiguous Grid Densities. *Theoritical and Computational Fluid Dynamics* 20, 181–195.

Troldborg, N., J. N. Sørensen and R. Mikkelsen (2008). *Actuator Line Modeling of Wind Turbine Wakes Printed in Denmark by DTU-Tryk, Lyngby.* Ph. D. thesis.